A Determination of the Intergalactic Redshift Dependent UV-Optical-NIR Photon Density Using Deep Galaxy Survey Data and the Gamma-ray Opacity of the Universe

Floyd W. Stecker

Astrophysics Science Division, NASA/Goddard Space Flight Center

Department of Physics and Astronomy, University of California, Los Angeles

Matthew A. Malkan

Department of Physics and Astronomy, University of California, Los Angeles

Sean T. Scully

Department of Physics, James Madison University

Received _____; accepted _____

ABSTRACT

We calculate the intensity and photon spectrum of the intergalactic background light (IBL) as a function of redshift using an approach based on observational data obtained in many different wavelength bands from local to deep galaxy surveys. This allows us to obtain an empirical determination of the IBL and to quantify its observationally based uncertainties. Using our results on the IBL, we then place 68% confidence upper and lower limits on the opacity of the universe to γ-rays, free of the theoretical assumptions that were needed for past calculations. We compare our results with measurements of the extragalactic background light and upper limits obtained from observations made by the *Fermi* Gamma-ray Space Telescope.

Subject headings: diffuse radiation – galaxies:observations – gamma rays:theory

1. Introduction

1.1. Empirical Approach to Determining the Intergalactic Background Radiation

The purpose of this paper is to present the results of a new, fully empirical approach to calculating the intergalactic background light (IBL) as well as the γ-ray opacity of the Universe. This methodology, hitherto unavailable, is now enabled by very recent data from deep galaxy surveys spanning the electromagnetic spectrum from millimeter to UV wavelengths and using galaxy luminosity functions for redshifts $0 \leq z \leq 8$ in the UV and for redshifts up to 2 or 3 in other wavelength ranges. We stress that this approach is both capable of *delineating empirically based uncertainties* on the determination of the IBL, and the γ-ray opacity of the Universe.

In this paper (Paper I) we specifically consider the frequency range from the far ultraviolet (FUV) to the near infrared I band (NIR), as this range is of particular relevance to the γ-ray opacity studies in the $\sim$0.1-200 GeV energy range being made by the *Fermi* γ-ray space telescope. A follow-up paper (Paper II) will address the frequency range from the NIR to the far-IR (FIR). That range has particular relevance for opacity studies by ground-based air Čerenkov telescopes.

Previous calculations the IBL at different redshifts have been based on various theoretical models and assumptions. These include backward evolution models (Malkan & Stecker 1998, 2001; Stecker, Malkan & Scully 2006; Franceschini et al. 2008), semi-analytical forward evolution models (*e.g.*, Gilmore et al. 2009; Somerville et al. 2011) and other models based on the evolution of galaxy parameters such as star formation rate and stellar population synthesis models (Salamon & Stecker 1998 (hereafter SS98); Kneiske et al. 2004). Kneiske & Dole (2010) have recently used a forward evolution model to derive lower limits on the EBL. Finke, Razzaque & Dermer (2010) employed a triple blackbody approximation to extimate the EBL. Domínguez et al. (2011) used an approach based on the redshift evolution of the K-band galaxy luminosity functions (LFs) derived by Cirasuolo et al. (2010), together with model templates based on *Spitzer*-based $0.2 \leq z \leq 1$ infrared galaxy SEDs and *AEGIS* data. To obtain K-band LFs for $1 < z < 4$, Cirasuolo et al. (2010) used 8 μm Spitzer/IRAC (Infrared Array Camera) channels combined with population synthesis models of Bruzual & Charlot (2003), including a correction for dust obscuration. Most recently, a semi-analytic model of the EBL has been published by Gilmore et el. (2012). The earlier exploration of the EBL using direct measurements, galaxy counts, and indirect constraints was reviewed some time ago by Hauser & Dwek (2001).

We note that previous studies had to adopt at least some assumptions about how galaxy LFs evolves with cosmic time, starting either at the present (well-measured epoch)

and going back in time, or starting with the simulations of the galaxy formation epoch using semi-analytic models (see above) or modeled galaxy SEDs. However, the latest observations have become sufficiently extensive and accurate to allow *direct integration* of observational data on galaxy LFs from the deep galaxy surveys at *many* wavelengths, where we can interpolate between observationally determined LFs at many wavelengths from the far UV to near infrared and the redshift range extending in the UV from $z = 0$ to $z \geq 8$. Thus, the first goal of our paper is to determine the IBL based on empirical data from deep survey galaxy observations. This avoids the complications entailed by theoretical calculations that have need of making various assumptions for stellar population synthesis models, stellar initial mass functions, unknown amounts of dust extinction, and poorly known stellar metallicity-age modeling for different evolving galaxy types (*e.g.*, Wilkins et al. 2012). This is because the observational data are the direct result of all of the physical processes involved in producing galactic emission. Thus our treatment only involves uncertainties inherent in the analyses discussed in the observational survey papers that we used.

1.2. Gamma Ray Opacity and the IBL

The second goal of our paper is to use our results on the IBL to determine the γ-ray opacity of the universe as a function of energy and redshift. It was first suggested by Stecker, De Jager & Salamon (1992) that γ-ray observations from high redshift sources such as blazars (and later γ-ray bursts) could be used to probe the IBL. Such studies make use of the opacity caused by the annihilation of γ-rays owing to interactions with low energy photons that produce e^+e^- pairs. The *Fermi Gamma-Ray Space Telescope (Fermi)* is now being used to probe the high redshift IBL at optical and UV wavelengths by constraining the opacity of the universe to multi-GeV γ-rays (Abdo et al. 2010). This is accomplished by measuring the energy of the highest energy photons observed by *Fermi* that have been

emitted by GRBs and blazars at known redshifts.

Observations of TeV γ-ray emitting blazars utilizing modern air Čerenkov telescope arrays also probe, or at least constrain, the nearby (redshift $z \sim 0 - 0.5$) intergalactic infrared background radiation. Attempts to constrain the IBL have been made by various authors (Stecker & de Jager 1993; Aharonian et al. 2006 (but see Stecker, Baring & Summerlin 2009); Mazin & Raue 2007; Georganopoulos, Fincke & Reyes 2010; Abdo et al. 2010; Orr, Krennrich & Dwek 2011, but see Stecker, Baring & Summerlin 2009).

Our methodology will also be used to define secure upper and lower limits on the opacity of the universe to high energy γ-rays based on the observational uncertainties in the deep survey data. We then compare the opacity range defined by these limits with the upper limits derived using the *Fermi* observations of multi-GeV γ-rays from high redshift sources Abdo, et al (2010).

2. Intergalactic Photon Energy Densities and Emissivities from Galaxies

The co-moving radiation energy density $u_\nu(z)$ is derived from the co-moving specific emissivity $\mathcal{E}_\nu(z)$, which, in turn is derived from the galaxy luminosity function (LF). The galaxy luminosity function, $\Phi_\nu(L)$, is defined as the distribution function of galaxy luminosities at a specific frequency or wavelength. The specific emissivity at frequency ν and redshift z (also referred to in the literature as the luminosity density, ρ_{L_ν}) , is the integral over the luminosity function

$$\mathcal{E}_\nu(z) = \int_{L_{min}}^{L_{max}} dL_\nu \, L_\nu \Phi(L_\nu; z) \tag{1}$$

There are many references in the literature where the LF is given and fit to Schechter parameters, but where ρ_{L_ν} is not given. In those cases, we could not determine the

covariance of the errors in the Schechter parameters used to determine the dominant statistical errors in their analyses. Thus, we could not ourselves accurately determine the error on the emissivity from equation (1). We therefore chose to use only the papers that gave values for $\rho_{L_\nu}(z) = \mathcal{E}_\nu(z)$ with errors. We did not consider cosmic variance, but this uncertainly should be minimized since we used data from many surveys.

In compiling the observational data on $\mathcal{E}_\nu(z)$, we scaled all of the results to a value of h = 0.7. Thus results using h = 0.5 were scaled by a factor of $(7/5)$[1].

The co-moving radiation energy density $u_\nu(z)$ is the time integral of the co-moving specific emissivity $\mathcal{E}_\nu(z)$,

$$u_\nu(z) = \int_z^{z_{\rm max}} dz'\, \mathcal{E}_{\nu'}(z') \frac{dt}{dz}(z') e^{-\tau_{\rm eff}(\nu,z,z')}, \tag{2}$$

where $\nu' = \nu(1+z')/(1+z)$ and $z_{\rm max}$ is the redshift corresponding to initial galaxy formation (Salamon & Stecker 1998, hereafter SS98), and

$$\frac{dt}{dz}(z) = [H_0(1+z)\sqrt{\Omega_\Lambda + \Omega_m(1+z)^3}]^{-1}, \tag{3}$$

with $\Omega_\Lambda = 0.72$ and $\Omega_m = 0.28$.

The opacity factor for frequencies below the Lyman limit is dominated by dust extinction. In the model of SS98, which relied on the population synthesis studies of Bruzual & Charlot (1993), dust absorption was not included. Our earlier paper (Stecker, Malkan & Scully 2006) used a rough approximation of the results obtained by Salamon & Stecker (1998) (SS98) and therefore, also did not take dust absorption into account. However, since we are here using actual observations of galaxies rather than models, dust

[1]Using the most recent and accurate value of 0.74 (Riess et al. 2011) would increase all of our results by $\sim 6\%$

absorption is implicitly included. The remaining opacity τ_ν refers to the extinction of ionizing photons with frequencies above the rest frame Lyman limit of $\nu_{LyL} \equiv 3.29 \times 10^{15}$ Hz by interstellar and intergalactic hydrogen and helium. It has been shown that this opacity is very high, corresponding to the expectation of very small fraction of ionizing radiation in intergalactic space compared with radiation below the Lyman limit (Lytherer et al.1995; SS98). In fact, the Lyman limit cutoff is used as a tool; when galaxies disappear when using a filter at a given waveband (*e.g.*, "U-dropouts", "V-dropouts") it is an indication of the redshift of the Lyman limit. We thus replace equation (2) with the following expression

$$u_\nu(z) = \int_z^{z_{\max}} dz' \, \mathcal{E}_{\nu'}(z') \frac{dt}{dz}(z') \mathcal{H}(\nu(z') - \nu'_{LyL}), \tag{4}$$

where $\mathcal{H}(x)$ is the Heavyside step function.

2.1. Empirical Specific Emissivities

2.1.1. Luminosity Densities

We have used the results of many galaxy surveys to compile a set of luminosity densities, $\rho_{L_\nu}(z) = \mathcal{E}_\nu(z)$ (LDs), at all observed redshifts, and at rest-frame wavelengths from the far-ultraviolet, FUV = 150 nm to the I band, I = 800 nm. Figure 1 shows the redshift evolution of the luminosity $\mathcal{E}_\nu(z)$ for the various wavebands based on those published in the literature.[2] The lower right panel shows all of the observational determinations of

[2]Table 1 references used to construct Figure 1 are as follows: Bouwens et al. (2007)(BO07), Bouwens et al. (2010)(BO10), Budavári et al.(2005)(BU05), Burgarella et al. (2007)(BU07), Chen et al.(2003) (CH03), Cucciati et al. (2012)(CU12), Dahlen et al. (2007)(DA07), Faber et al. (2007)(FA07) and references therein, Iwata et al. (2007)(IW07), Ly et al. (2009)(LY09),

galaxy LDs from the references in footnote 2. The specific waveband and mean redshift identifications for these data are listed in Table 1 using the key abbreviations indicated in footnote 2. This table reflects the fact that direct determinations of galaxy LDs are only available out to an *observed wavelength* of about 2.2 μm (rest wavelength $2.2/(1+z)$ μm). This is because any attempt to survey large areas of the sky with ground-based telescopes in wavebands longer than 2μm is prevented by the sudden increases in background noise.[3]

Thus, at redshifts above 1.6, the longest rest-wavelengths under consideration no longer have well measured LDs. At these longer wavelengths, we are obliged to fall back on a secondary method for estimating galaxy luminosities: we use the closest available LDs, and extrapolate them using the average observed *color* of galaxies from measurements at that redshift. This 'minimal extrapolation' should be reliable because the average galaxy colors, especially at long wavelengths, change only gradually with redshift. For example, the galaxies that are included in the rest-frame R band LD at $z = 2.2$ by Marchesini et al. are very similar to those of the galaxies that would have been included in an I-band LD at that redshift. Since we are only extrapolating by a small step in wavelength ($\Delta\lambda/\lambda \sim 0.15$),

---

Reddy & Steidel (2009)(RE09), Marchesini et al. (2007)(MA07), Marchesini & Van Dokkum 2007 (MAV07), Marchesini et al. (2012)(MA12), Oesch et al. (2010)(OE10), Paltani et al. (2007)(PA07), Reddy et al. (2008)(RE08), Sawicki & Thompson (2006)(SA06), Schiminovich et al. (2005)(SC05), Steidel et al. (1999)(ST99), Tresse et al. (2007) (TR07), Wolf et al.(2003) (WO03), Wyder et al. (2005)(WY05), Yoshida et al. (2006)(YO06).

[3]This 2μm barrier is only circumvented by using space-based mid-infrared (3 to 8μm) telescopes such as *AKARI* (with its Infrared Camera, IRC), and *Spitzer* (with its Infrared Array Camera, IRAC). These telescopes have only conducted multi-band imaging and redshift surveys with the necessary sensitivity to measure the high-redshift ($z \geq 2$) galaxy population in a few, relatively small deep fields.

it is quite reasonable to shift the R-band LD using the average $R - I$ colors observed at that redshift. The incremental color shifts we apply become large only at $z \geq 4$, where, as we show in Section 4, the overall contributions to the IBL γ-ray opacity are not very substantial. Our color relations, which are also used to interpolate between the closely spaced wavebands, are given the next subsection. They are given as a function of redshift, z, since galaxies tend to be bluer on average at higher redshifts.

2.1.2. Average Colors

It is hardly surprising that there are often large apparent jumps, or changes, in the shape and the normalization of the LDs going from one waveband to an immediately adjacent one. We therefore applied an independent test of the consistency of these LDs, by comparing the integrated *ratios* of LDs at adjacent wavebands to the published average colors measured by observers. This test has the great advantage of not requiring accurate estimates of volume incompleteness or even very accurate redshifts. Broadband colors (*i.e.,* local continuum slopes) are easier to measure than LDs. The main problem is that all galaxy samples at all redshifts show a wide observed range of broadband colors. The typical 1σ scatter we found in published color distributions was $\pm$ 0.5 mag. A few rest-frame colors that are very sensitive to stellar population, such as $U - B$, often show even larger variation.

In order to determine the redshift evolution of the LD in each of the bands out to a redshift of $\sim$ 8, we utilized color relations to transform data from other bands. We have chosen to include all data possible in excess of $z = 1.5$ to fill in the gaps for various wavebands mostly at higher redshifts.[4]. This also provides both an overlap to existing data

[4]The most comprehensive observations of galaxies in the best observed Deep Fields include extremely sensitive Spitzer/IRAC photometry. The IRAC data are most complete in

and multiple sources of data as a check for consistency of our color relations.

Published estimates of *average colors* from galaxy surveys at various wavebands and redshifts tend to be bluer at shorter wavelengths, and redder at longer wavelengths. This is due to the composite nature of stellar populations in galaxies, with hot young stars making a stronger contribution in the UV portion of the spectrum while red giants dominate the long wavelengths. Thus, the galaxies that are included in a UV LF and not all the same galaxies as those included in an LF in the R band.

There is a clear trend with redshift over all wavelengths, which is well known. Redder galaxies (*e.g.*, local E and S0 galaxies) are more and more outnumbered by blue, actively star-forming galaxies, at higher redshifts. The average characteristic age of stellar populations decreases with redshift. Our color relations agree with this trend. At the highest redshifts most known galaxies are dominated by young starburst populations of O and B stars. This tends to produce very blue overall spectral energy distribution without very much sensitivity to the exact details of the star formation. These factors are automatically taken into account when one uses the actual observational data on the LDs at various wavelengths and redshifts.

Defining the average wavelengths of the various bands in nm as follows:

FUV = 150, NUV = 280, U = 365, B = 445, V = 551, R = 658, I = 806 nm

We then use the commonly measured astronomical parameter β, which is defined by the relation between the differential flux and wavelength of a galaxy, $f_\lambda \propto \lambda^\beta$. We have adopted the following relations (colors) for $\beta_{\Delta\lambda}(z)$:

---

its Band 1 (3.6 μm observed) wavelength, and gradually become less sensitive out to the reddest IRAC band at 8 μm observed wavelength corresponding to a rest wavelength of $8/(1+z)$ μm.

$$\beta(FUV - NUV) = -1.0 - 1.25log(1+z),\ log(1+z) \leq 0.8$$

derived from Bouwens, et al. (2009); Budavári et al.(2005); Castellano et al. (2012); Cucciati, et al. (2012); Dunlop et al. (2012); Willott, et al. (2012); Wyder et al.(2005),

$$\beta(B - V) = +0.3 - 1.6log(1+z),\ log(1+z) \leq 0.6$$

derived from Arnouts et al.(2007); Brammer (2011),

$$\beta(NUV - U) = +0.5 - 1.2log(1+z),\ log(1+z) \leq 0.6$$

derived from Tresse et al. (2007),

$$\beta(NUV - R) = +2.5 - 6.0log(1+z),\ log(1+z) \leq 0.6$$

$$\beta(U - V) = +1.3 - 3.0log(1+z),\ log(1+z) \leq 0.6$$

derived from Arnouts, et al. (2007); Brammer (2011): Ly et al. (2009),

$$\beta(U - B) = +3.0 - 5.0log(1+z),\ log(1+z) \leq 0.6$$

derived from Marchesini et al. (2007); González et al. (2011),

For the FUV-NUV relation we set $\beta[log(1+z) > 0.8] = \beta[log(0.8)]$. For all of the other relations we set $\beta[log(1+z) > 0.6] = \beta[log(0.6)]$.

We used the above redshift-dependent relations where appropriate in our analysis. We stress that in the redshift ranges where they overlap, *the colored (observational) data points shown for the various wavelength bands in Figure 1 agree quite well, within the uncertainties, with the black data points that were extrapolated from the shorter wavelength bands using our color relations.* Also, where there is no overlap at the higher redshifts, the uncertainty bands in photon density (see next section) show no discontinuities.

2.2. Photon Density Calculations

The observationally determined LDs, combined with the color relations, extend our coverage of galaxy photon production from the FUV to the NIR in the galaxy rest frame. We have at least one or two determinations at each wavelength across the most crucial redshift range $0 \leq z \leq 2.5$. However, to calculate the opacity for photons at energies higher than $\sim 250/(1+z)$ GeV (see next section), requires the determination of galaxy LDs at longer rest wavelengths and higher redshifts. These regimes are less well constrained by observations, since they require measurement of very faint galaxies at long wavelengths (mid-IR observed frame.) We will address this topic further in Paper II. We have assumed a constant color at high redshift at the longer wavelengths as stated above. However, we stress that our final results are not very sensitive to errors in our average color relations because the interpolations that we make cover very small fractional wavelength intervals, $\Delta\lambda(z)$. We have directly tested this by numerical trial.

The second goal of our paper is to place upper and lower limits (within a 68% confidence band) on the opacity of the universe to γ-rays . These limits are a direct result of the 68% confidence band upper and lower limits of the IBL determined from the observational data on ρ_{L_ν} . In order to determine these limits, we make no assumptions about the luminosity density evolution. We derive a luminosity confidence band in each waveband by using a robust rational fitting function characterized by

$$\rho_{L_\nu} = \mathcal{E}_\nu(z) = \frac{ax+b}{cx^2+dx+e} \tag{5}$$

where $x = \log(1+z)$ and a,b,c,d,and e are free parameters.

The 68% confidence band is then computed from Monte Carlo simulation by finding 100,000 realizations of the data and then fitting the rational function. In order to best represent the tolerated confidence band, particularly at the highest redshifts, we have

chosen to equally weight all FUV points in excess of a redshift of 2. Our goal is not to find the best fit to the data but rather the limits tolerated by the current observational data. In order to perform the Monte Carlo of the fitting function, a likelihood is determined at each redshift containing data. The shape of the function is taken to be Gaussian (or the sum of Gaussians where multiple points exist) for symmetric errors quoted in the literature. Where symmetric errors are not quoted it is impossible to know what the actual shape of the likelihood functions is. We have chosen to utilize a skew normal distribution to model asymmetric errors. This assumption has very little impact on the determination of the confidence bands. The resulting bands are shown along with the luminosity density data in Figure 1.

With the confidence bands established, we take the upper and lower limits of the bands to be our high and low IBL respectively. We then interpolate each of these cases separately between the various wavebands to find the upper and lower limit rest frame luminosity densities. The calculation is extended to the Lyman limit using the slope derived from our color relationship between the near and far UV bands.

The specific emissivity is then the derived high and low IBL luminosity densities $\mathcal{E}_\nu(z) = \rho_{L_\nu}(z)$. The co-moving radiation energy density is determined from equation 4. Figure 2 shows the resulting photon density determined by dividing the energy density by the energy in each frequency for high and low IBL. This result is used as input for the determination of the optical depth of the universe to γ-rays .

The photon densities

$$\epsilon n(\epsilon, z) = u(\epsilon, z)/\epsilon \quad , \tag{6}$$

with $\epsilon = h\nu$, as calculated using equation (2), are shown in Figure 2.

3. Comparison of z = 0 IBL with Data and Constraints

As a byproduct of our determination of the IBL as a function of redshift using LDs from galaxy surveys, we have also determined the local ($z = 0$) IBL, also known as the extragalactic background light (EBL). Determining the EBL directly has been the object of intense observational effort, although the various estimates and limits in the published literature are far from consistent with each other. Nonetheless, since these observations provide a potential consistency check on our calculations, we consider them here.

Using equation (2), together with our empirically based determinations given the confidence band derived for our specific emissivities, $\mathcal{E}_\nu(z)$, we have evaluated the EBL within the 68% confidence band upper and lower limits within the wavelength range of our calculations. This band is indicated by the gray zone in Figure 3. We also show recent measurements using the Hubble Wide-field Planetary Camera 2 (Bernstein 2007), the dark field from Pioneer 10/11 (Matsuoka et al. 2011) and the preliminary analysis of Mattila et al. (2011) using differential measurements using the ESO VLT (very large telescope array). Figure 3 also shows the various lower limits from galaxy counts obtained by Gardner et al. (2000) from the ST Imaging Spectrograph data, by Madau & Pozzetti (2000) using Hubble Deep Field South data, and by Xu et al. (2005) from GALEX (Galaxy Evolution Explorer) data, all indicated by upward-pointing arrows.

4. The Optical Depth from Interactions with Intergalactic Low Energy Photons

The cross section for photon-photon scattering to electron-positron pairs can be calculated using quantum electrodynamics (Breit & Wheeler 1934). The threshold for this interaction is determined from the frame invariance of the square of the four-momentum

vector that reduces to the square of the threshold energy, s, required to produce twice the electron rest mass in the c.m.s.:

$$s = 2\epsilon E_\gamma(1 - \cos\theta) = 4m_e^2 \tag{7}$$

This invariance is known to hold to within one part in 10^{15} (Stecker & Glashow 2001; Jacobson, Liberati, Mattingly & Stecker 2004).

With the co-moving energy density $u_\nu(z)$ evaluated, the optical depth for γ-rays owing to electron-positron pair production interactions with photons of the stellar radiation background can be determined from the expression (Stecker, De Jager, & Salamon 1992)

$$\tau(E_0, z_e) = c\int_0^{z_e} dz\,\frac{dt}{dz}\int_0^2 dx\,\frac{x}{2}\int_0^\infty d\nu\,(1+z)^3\left[\frac{u_\nu(z)}{h\nu}\right]\sigma_{\gamma\gamma}[s = 2E_0 h\nu x(1+z)], \tag{8}$$

In equations (7) and (8), E_0 is the observed γ-ray energy at redshift zero, ν is the frequency at redshift z, z_e is the redshift of the γ-ray source at emission, $x = (1 - \cos\theta)$, θ being the angle between the γ-ray and the soft background photon, h is Planck's constant, and the pair production cross section $\sigma_{\gamma\gamma}$ is zero for center-of-mass energy $\sqrt{s} < 2m_e c^2$, m_e being the electron mass. Above this threshold, the pair production cross section is given by

$$\sigma_{\gamma\gamma}(s) = \frac{3}{16}\sigma_{\rm T}(1-\beta^2)\left[2\beta(\beta^2-2) + (3-\beta^4)\ln\left(\frac{1+\beta}{1-\beta}\right)\right], \tag{9}$$

where σ_T is the Thompson scattering cross section and $\beta = (1 - 4m_e^2c^4/s)^{1/2}$ (Jauch & Rohrlich 1955).

It follows from equation (7) that the pair-production cross section energy has a threshold at $\lambda = 4.75\ \mu\mathrm{m} \cdot E_\gamma(\mathrm{TeV})$. Since the maximum λ that we consider here is in the rest frame I band at 800 nm at redshift z, and we observe E_γ at redshift 0, so that its

energy at interaction in the rest frame is $(1+z)E_\gamma$, we then get a conservative upper limit on E_γ of $\sim 200(1+z)^{-1}$ GeV as the maximum γ-ray energy affected by the photon range considered here. Allowing for a small error, our opacities are good to $\sim 250(1+z)^{-1}$ GeV. The 68% opacity ranges for $z = 0.1, 0.5, 1, 3$ and 5, calculated using equation (8) are plotted in Figure 4.

The widths of the grey uncertainty ranges in the LDs shown in Figure 1 increase towards higher redshifts, especially at the longest rest wavelengths. This reflects the decreasing amount of long-wavelength data and the corresponding increase in uncertainties about the galaxies in those regimes. However, these uncertainties do not greatly influence the opacity calculations. Because of the short time interval of the emission from galaxies at high redshifts their photons do not contribute greatly to the opacity at lower redshifts. Indeed, Figure 4 shows that the opacities determined for redshifts of 3 and 5 overlap within the uncertainties.

5. Results and Implications

We have determined the IBL using local and deep galaxy survey data, together with observationally produced uncertainties, for wavelengths from 150 nm to 800 nm and redshifts out to $z > 5$. We have presented our results in terms of 68% confidence band upper and lower limits. As expected, our $z = 0$ (EBL) 68% lower limits are higher than those obtained by galaxy counts alone, since the EBL from galaxies is not completely resolved. Our results are also above the theoretical lower limits given recently by Kneiske and Dole (2010). In Figure 3, we compare our $z = 0$ result with both published and preliminary measurements and limits.

Figure 5 shows our 68% confidence band for $\tau = 1$ on an energy-redshift plot compared

with the *Fermi* data on the highest energy photons from extragalactic sources at various redshifts as given by Abdo et al. (2010). It can be seen that none of the photons from these sources would be expected to be significantly annihilated by pair production interactions with the IBL. This point is brought out further in Figure 6. This figure compares the 68% confidence band of our opacity results with the 95% confidence upper limits on the opacity derived for specific blazars by Abdo et al. (2010).

For purposes of discussion, we mention some points of comparison with previous work. Our EBL results for $z = 0$, while lower than the fast evolution model of our previous work, are generally higher than those modeled more recently. As an example, at a wavelength of 200 nm in the FUV range our uncertainty range is a factor of 1.8 - 4.2 higher than the recent fiducial semi-analytic model of Gilmore et al. (2012) and similarly higher than the previous model result of Dominguez et al. (2011). Our opacity results at $z \simeq 1$ are comparable to, or lower than, the models of Kneiske et al. (2004). They are also consistent with the results of the non-metallicity corrected model of SS98. However, they are higher than the models of Franceschini et al. (2008), Gilmore et al. (2009), and Finke et al. (2010), as indicated by comparing Figure 3 of Abdo et al. (2010) with our Figure 5. We stress that these comparisons are for illustrative purposes only. Because our new methodology is based on the direct use of luminosity densities derived directly from observations, we take the position that they stand by themselves and should be compared primarily with the observational data as shown in our Figures 3, 5 and 6. In that regard, we find full consistency within our observationally determined uncertainties.[5]

[5]While we were preparing our revised manuscript for publication a similar empirically based calculation by Helgason & Kashlinsky (2012) appeared on the arXiv. These authors calculated the EBL and γ-ray opacity based on galaxy luminosity functions compiled by Helgason, Ricotti & Kashlinsky (2012) extrapolated to $z \geq 2$ using an exponential cutoff in

Our result bears on questions regarding the possible modification of the pair-production opacity effect on the γ-ray flux from distant extragalactic sources, either by line-of-sight photon-axion oscillations during propagation (*e.g.*, De Angelis et al. 2009) or by the addition of a component of secondary γ-rays from interactions of blazar-produced cosmic-rays with photons along the line-of-sight to the blazar (*e.g.*, Essey et al. 2010; Essey & Kusenko 2012). Future theoretical studies and future γ-ray observations of extragalactic sources with *Fermi* and the *Čerenkov Telescope Array*, which will be sensitive to extragalactic sources at energies above 10 GeV (Gernot 2011), should help to clarify these important aspects of high energy astrophysics.

6. Our Results Online

Our results in numerical form are available at the following link:

http://csma31.csm.jmu.edu/physics/scully/opacities.html

Acknowledgments

We would like to thank Luis Reyes and Anita Reimer for supplying us with the Fermi results shown in Figure 5. We thank Richard Henry for a helpful discussion of the UV background data. We also thank Tonia Venters for helpful discussions. This research was partially supported by a NASA Astrophysics Theory Grant and a NASA Fermi Guest Investigator Grant.

---

z. Their opacity results are generally consistent with the results presented here.

REFERENCES

Abdo, A., Ackermann, M., Ajello, M. et al. 2010, ApJ, 723, 1082

Aharonian, F. et al. 2006, Nature, 440, 1018

Arnouts, Schiminovich, D., Libert, O. et al 2005, ApJ, 619, L43

Arnouts, S. and Walcher, C. J. and Le Fèvre, O. et al. 2007, A&A, 476, 137

Bertin, E., & Arnouts, S. 1996, A&AS, 117, 393

Bernstein, R. A. 2007, ApJ, 666, 663

Blanton, M. R., Hogg, D. W. , Bahcall, N.A. et al. 2003, ApJ, 592, 819

Bouwens, R.J., Illingworth, G.D., Franx, M. & Ford, H. 2007, ApJ, 670, 928

—. 2008, ApJ, 686, 230

Bouwens, R.J., Illingworth, G. D. Franx, M. et al. 2009, ApJ, 705, 936

Bouwens, R. J., Illingworth, G. D., Oesch, P. A. et al. 2010, ApJ, 709, L133

Bouwens, R. J., Illingworth, G. D., Oesch, P. et al. 2011, ApJ, 737:90

Brammer, G. B., Whitaker, K.E., van Dokkum, P.G., Marchesini, D. et al. 2011, ApJ, 739, 24

Breit, G and Wheeler, J.A. 1934, Phys. Rev. 46, 1087

Bruzual, G., & Charlot, S. 2003, MNRAS, 344, 1000

Budavári, T., Szalay, A.S., Charlot, S. et al. 2005, ApJ, 619, L31

Bunker, A. J., Wilkins, S., Ellis, R. S. et al. 2010, MNRAS, 409, 855

Burgarella, D., Pérez-González, P. G., Tyler, K. D. et al. 2007, MNRAS, 380, 986

Capak, P., Aussel, H., Ajiki, M., et al. 2007, ApJS, 172, 99

Castellano, M. Fontana, A., Grazian, A. et al. 2012, A&A, 540, 39

Chary, R. & Elbaz, D. 2001, ApJ, 556, 562

Chen, H.-W., Marzke, R.O., McCarthy, P.J. et al. 2003, ApJ, 586, 745

Cirasuolo, M., McLure, R.J., Dunlop, J.S. et al. 2010, MNRAS, 401, 1166

Cohen, J. G., Hsieh, S., Metchev, S., Djorgovski, S. G. & Malkan, M. 2007, AJ 133, 99

Cucciati, O. Tresse, L., Ilbert, O. et al. 2012, A&A 539, A31

Dahlen, T. Mobasher, B., Somerville, R. S. et al. 2005, ApJ 631, 126

Dahlen, T. Mobasher, B., Dickinson, M. et al. 2007, ApJ 654, 172

Dunlop, J.S., McLure, R. J., Robertson, B. E. et al. 2012, MNRAS 420, 901

De Angelis, A., Mansutti, O., Persic, M. & Roncadelli, M. 2009 MNRAS 394, L21

Domínguez, A. 2011, arXiv:1111.4435

Domínguez, A., Primack, J. R., Rosario, D. J. et al. 2011, MNRAS 410, 2556

Essey, W., Kalashev, O. E., Kusenko, A. and Beacom, J. F. 2010, Phys. Rev. Letters 104, 141102

Essey, W. & Kusenko, A. 2012, ApJ 751, L11

Faber, S.M., Willmer, C.N.A., Wolf, C. et al. 2007, ApJ, 665, 265

Fazio, G. G. & Stecker, F. W. 1970, Nature 226, 135

Finke, J. D., Razzaque, S. & Dermer, C. D. 2010, ApJ 712, 238

Franceschini, A., Rodighiero, G. & Vaccari, M. 2008, A&A, 487, 837

Gardner, J. P., Brown, T. M. & Ferguson, H. C. 2000, ApJ, 542, L79

Gernot, M. 2011, in *Proc. XMM Science Workshop, Berlin*, article 098

Georganopoulos, M, Fincke, J.D. & Reyes, L.C. 2010, ApJ, 714, L57

Giavalisco, M., Dickinson, M., Ferguson, H. C. et al. 2004, ApJ, 600, L103

Gilmore, R. C. and Madau, P., Primack, J. R.,Somerville, R. S.& Haardt, F. 2009, MNRAS, 399, 1694

Gilmore, R. C., Somerville, R. S., Primack, J. R. & Dominguez 2012, MNRAS, 422, 3189

González, V., Bouwens, R., Labbe, I. et al. 2011, arXiv:1110.6441

Hathi, N. P., Ryan, R.E., Jr.; Cohen, S.H. et al. 2010, ApJ, 720, 1708

Hauser, M. & Dwek, E. 2001, Ann. Rev. Astron. Astrophys. 39, 249

Heath-Jones, D., Peterson, B., Colless, M. & Saunders, W. 2006, MNRAS, 369, 25

Helgason, K. & Kashlinsky, A. 2012, arXiv:1208.4364

Helgason, K., Ricotti, M. & Kashlinsky, A. 2012, ApJ, 752:113

Hewett, P.C., Warren, S.J., Leggett, S.K, & Hodgkin, S.T. 2006 MNRAS, 367, 454

Hill, D.T., Driver, S.P., Cameron, E. et al. 2010, MNRAS 404, 1215

Hill, M.D. & Shanks, T. 2011, MNRAS, 414, 1875

Ilbert, O., Lauger S., Tresse, L. et al. 2006, A&A 453, 809

Iwata, I., Ohta, K., Tamura, N. et al. 2007, MNRAS, 376, 1557

Jacobson, T., Liberati, S., Mattingly, D., & Stecker, F. W. 2004, Phys. Rev. Lett., 93, 021101

Kneiske, T. M., Bretz, T., Mannheim, K. & Hartmann, D. H. 2004, A&A, 413, 807

Kneiske, T. M. & Dole, H. 2010, A&A, 515, A19

Leitherer, C., Ferguson, H. C., Heckman, T. M. et al. 1995, ApJ 454, L19

Ly, C., Malkan, M. A., Treu, T., et al. 2009, ApJ, 697, 1410

Madau, P. 1995, ApJ, 441, 18

Madau, P. & Pozzettti, L. 2000, MNRAS 312, L9

Magnelli, B., Elbaz, D.; Chary, R. R.et al. 2011, A&A, 528, A35

Malkan, M.A. & Stecker, F.W. 1998, ApJ, 496, 13

— 2001, ApJ, 555, 641

Marchesini D. & van Dokkum, P. 2007, ApJ 663, L89

Marchesini, D., van Dokkum, P. Quadri, R et al. 2007, ApJ, 656, 42

Marchesini, D., Stefanon, M., Brammer, G.B. & Whitaker, K.E. 2012, ApJ, 748, 126

Matsuoka, Y., Ienaka, N., Kawara, K. and Oyabu, S. 2011, ApJ, 736:119

Mattila, K. Lehtinen, K. Väisänen, P. et al. 2011, arXiv:1111.6747

Mazin, D. & Raue, M. 2007, A&A, 471, 439

McLure, R. J., Cirasuolo, M., Dunlop, J. S. et al. 2009, MNRAS, 395, 2196

McLure, R. J., Dunlop, J. S., Cirasuolo, M. et al. 2010, MNRAS, 403, 960

Oesch, P. A., Bouwens R. J., Carollo, C. M. et al.2010 ApJ, 725, L150

Orr, M.R, Krennrich, F. & Dwek, E. 2011, ApJ, 733, 77

Ouchi, M., Mobasher, B., Shimasaku, K. et al. 2009, ApJ, 706, 1136

Palatini, S., Le Fevre, Ilbert, O. et al. 2007, A&A, 463, 873

Reddy, N. A., & Steidel, C. C. 2009, ApJ, 692, 778

Reddy, N. A., Steidel, C.C., Pettini, M. et al. 2008, ApJS, 175, 48

Riess, A. G., Macri, L., Casertano, S. et al. 2011, ApJ 730, 119

Robotham, A.S.G & Driver, S.P. 2011, MNRAS 413, 2570

Salamon, M.H. & Stecker, F.W. 1998 (SS98), ApJ, 493, 547

Sawicki, M., & Thompson, D. 2006, ApJ, 648, 299

Schechter, P. 1976, ApJ, 203, 297

Schiminovich, D., Ilbert, O., Arnouts, S. et al. 2005, ApJ, 619, L47

Schmidt, M. 1968, ApJ, 151, 393

Somerville, R. S., Gilmore, R. C., Primack, J. R. & Dominguez, A. 2011, arXiv:1104.0669

Stefanon, M. & Marchesini, D. 2011, arXiv:1112.0006

Stecker, F.W. 1969, ApJ, 157, 507

Stecker, F.W., De Jager, O.C. & Salamon, M.H. 1992, ApJ, 390, L49

Stecker, F.W. & De Jager, O.C. 1993, ApJ 415, L71

Stecker, F.W. & Glashow, S. L. 2001, Astropart. Phys. 16, 97

Stecker, F.W., Malkan, M.A. & Scully, S.T. 2006, ApJ, 648, 774

Steidel, C. C., Adelberger, K. L.; Giavalisco, M. et al. 1999, ApJ, 519, 1

Tresse, L., Ilbert, O., E. Zucca, E. et al. 2007, A&A, 472, 403

Treyer, M. A., et al. 1998, MNRAS, 300, 303

Wilkins, S.M., Bunker, A. J., Stanway, E. et al. 2011, MNRAS 417, 717

Wilkins, S.M., Gonzalez-Perez, V., Lacey, C.G. and Baugh, C.M. 2012, arXiv:1206.2732

Willott, C. J., McLure, R. J., Hibon, P. et al., arXiv:1202.5330

Williams, R. J., Quadri, R. F., Franx, M. et al. 2009 ApJ 691, 1879

Wuyts, S., Labbe, I., Franx, M. et al. 2007 ApJ 655, 51

Wyder, T. K., Treyer, M.A., Milliard, B., et al. 2005, ApJ, 619, L15

Xu, C. K., Donas, J., Arnouts, S. et al. 2005, ApJ, 619, L11

Yoshida, M., Shimasaku, K., Kashikawa, N. et al. 2006, ApJ, 653, 988

This manuscript was prepared with the AAS LaTeX macros v5.0.

Table 1. Identification of References for Fig. 1 Data by Waveband and Redshift

z	FUV	NUV	U	B	V	R	I
.05	SC05, WY05	WY05					
.1	BU05,CU12	BU05,CU12					
.15	TR07	TR07	TR07	TR07	TR07	TR07	TR07
.20	BU05	BU05					
.25	WO03	WO03				WO03	
.3	SC05,CU12,SC05,TR07	TR07,CU12	TR07,DA05	TR07,DA05,FA07	TR07	TR07	TR07
.35		DA07, WO03		WO03		WO03	
.45		WO03	DA05	DA05, WO03		WO03	
.5	SC05, CU12, TR07	TR07	TR07	TR07, FA07	TR07	TR07	TR07
.55		DA07, WO03		WO03		WO03	
.6			DA05	DA05		CH03	
.65		WO03		WO03	MA12	WO03	
.7		TR07,CU12	TR07	TR07, FA07	TR07	TR07	TR07
.75		WO03		WO03		WO03	
.85		WO03		WO03		WO03	
.9	TR07,CU12	TR07,CU12	TR07, DA05	TR07, DA05, FA07	TR07	TR07	TR07
.95		WO03	DA05	WO03, DA05	MA12	WO03, DA05	
1.0	SC05	WO03		WO03		WO03	
1.1	CU12, TR07, DA07, BU07	DA07,TR07,CU12, WO03	TR07	TR07, FA07, WO03	TR07	TR07, WO03	TR07
1.2			DA05	DA05		CH03, DA05	
1.3	CU12, TR07	TR07	TR07	TR07	TR07	TR07	TR07
1.4	CU12	CU12					
1.5			DA05	DA05		DA05	
1.6	TR07	TR07	TR07	TR07	TR07	TR07	TR07
1.7			DA05	DA05		DA05	
1.8	DA07	DA07			MA12		
1.9			DA05	DA05		DA05	
2.0	SC05						
2.1	CU12	CU12					
2.2	RE08, SA06			MA07	MA07	MA07	
2.3	LY09						
2.4					MA12		
2.9	SC05						
3.0	CU12	CU12		MA07	MA07, MA12		
3.5	PA07						
3.8	BO07				MA12		
4.0	YO06,CU12						
4.1	SA06						
4.8	IW07						
5.0	BO07						
5.9	BO07						
6.8	BO11						
7.0	OE10						
8.2	BO10						

Figure Captions

Figure 1: The observed specific emissivities in our fiducial wavebands. The lower right panel shows all of the observational data from the references in footnote 1. In the other panels, non-band data have been shifted using the color relations given in the text in order to fully determine the specific emissivities in each waveband. The symbol designations are FUV: black filled circles, NUV: magenta open circles, U: green filled squares, B: blue open squares, V: brown filled triangles, R: orange open triangles, I: yellow open diamonds. Grey shading: 68% confidence bands (see text).

Figure 2: The photon densities $\epsilon n(\epsilon)$ shown as a continuous function of photon energy and redshift for both the high (upper panel) and low (lower panel) IBL.

Figure 3: Our empirically-based determination of the EBL together with lower limits and data as described in the text. The legend is as follows: Madau & Pozzetti(2000):Black Cicles, Xu et al.(2005):Crosses, Gardner et al.(2000):Open Squares, Matsuoka et al.(2011):Open Circles, Mattilla et al.(2011)(preliminary):Black Squares, Bernstein(2007):Black Diamonds. The upper limit from Mattilla et al.(2011) is thickened for clarity.

Figure 4: Our empirically determined opacities for redshifts of 0.1, 0.5, 1, 3, 5. The dashed lines are for $\tau = 1$ and $\tau = 3$.

Figure 5: A $\tau = 1$ energy-redshift plot (Fazio & Stecker 1970) showing our uncertainty band results compared with the *Fermi* plot of their highest energy photons from FSRQs (red), BL Lacs (black) and and GRBs (blue) *vs.* redshift (from Abdo et al. 2010).

Figure 6: Our opacity results for the redshifts of the blazars compared with 95% confidence opacity upper limits (red arrows) and 99% confidence limits (blue arrows) as given by the

Fermi analysis of Abdo, et al. (2010).

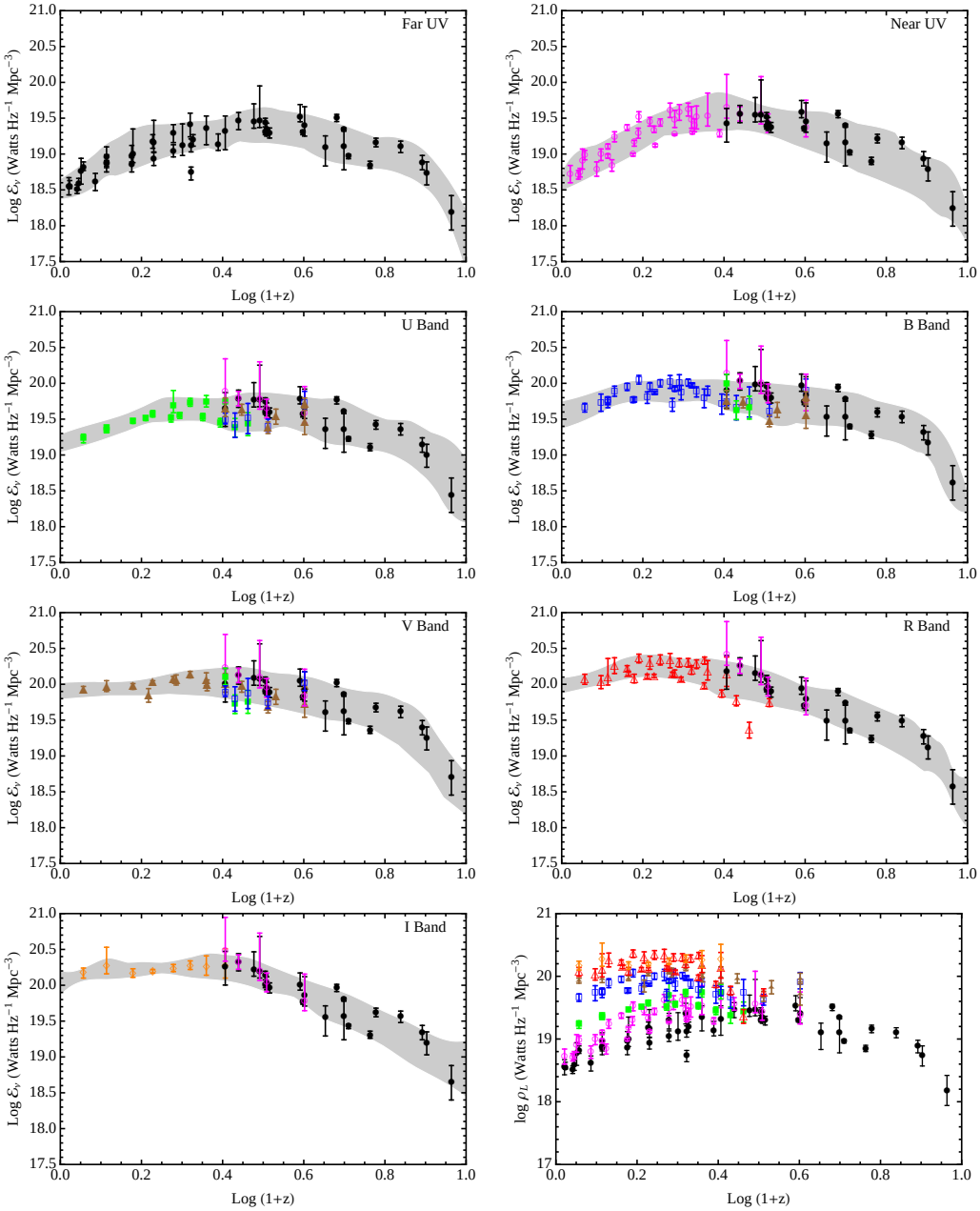
Far UV
Near UV
U Band
B Band
V Band
R Band
I Band
Log $\mathcal{E}_\nu$ (Watts Hz^{-1} Mpc^{-3})
log ρ_L (Watts Hz^{-1} Mpc^{-3})
Log (1+z)

Figure 1.

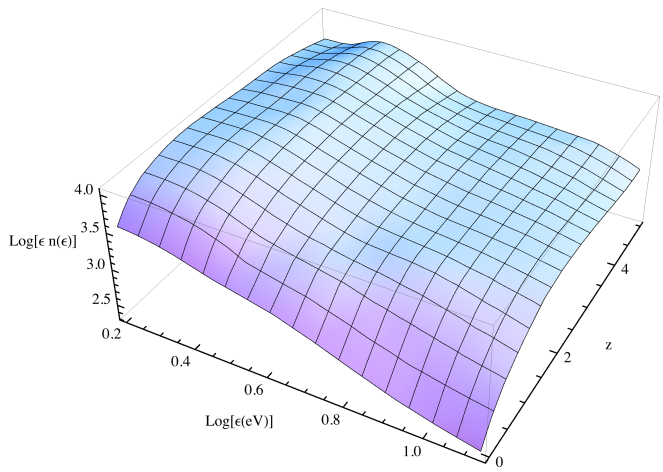
4.0
3.5
Log[ϵ n(ϵ)]
3.0
2.5
0.2
0.4
0.6
Log[ϵ(eV)]
0.8
1.0
0
2
z
4

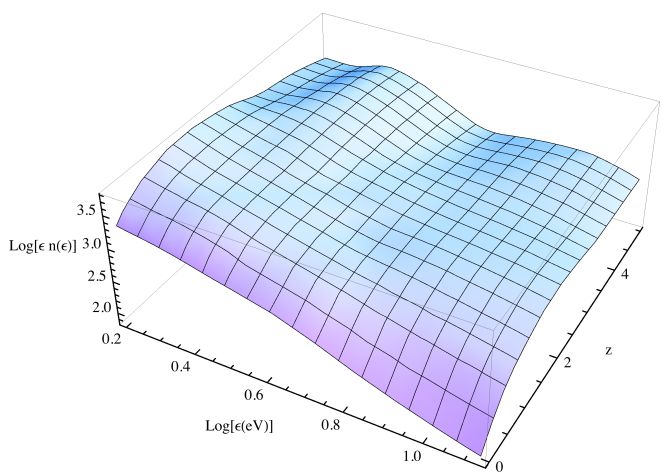
3.5
Log[ϵ n(ϵ)]
3.0
2.5
2.0
0.2
0.4
0.6
Log[ϵ(eV)]
0.8
1.0
0
2
z
4

Figure 2.

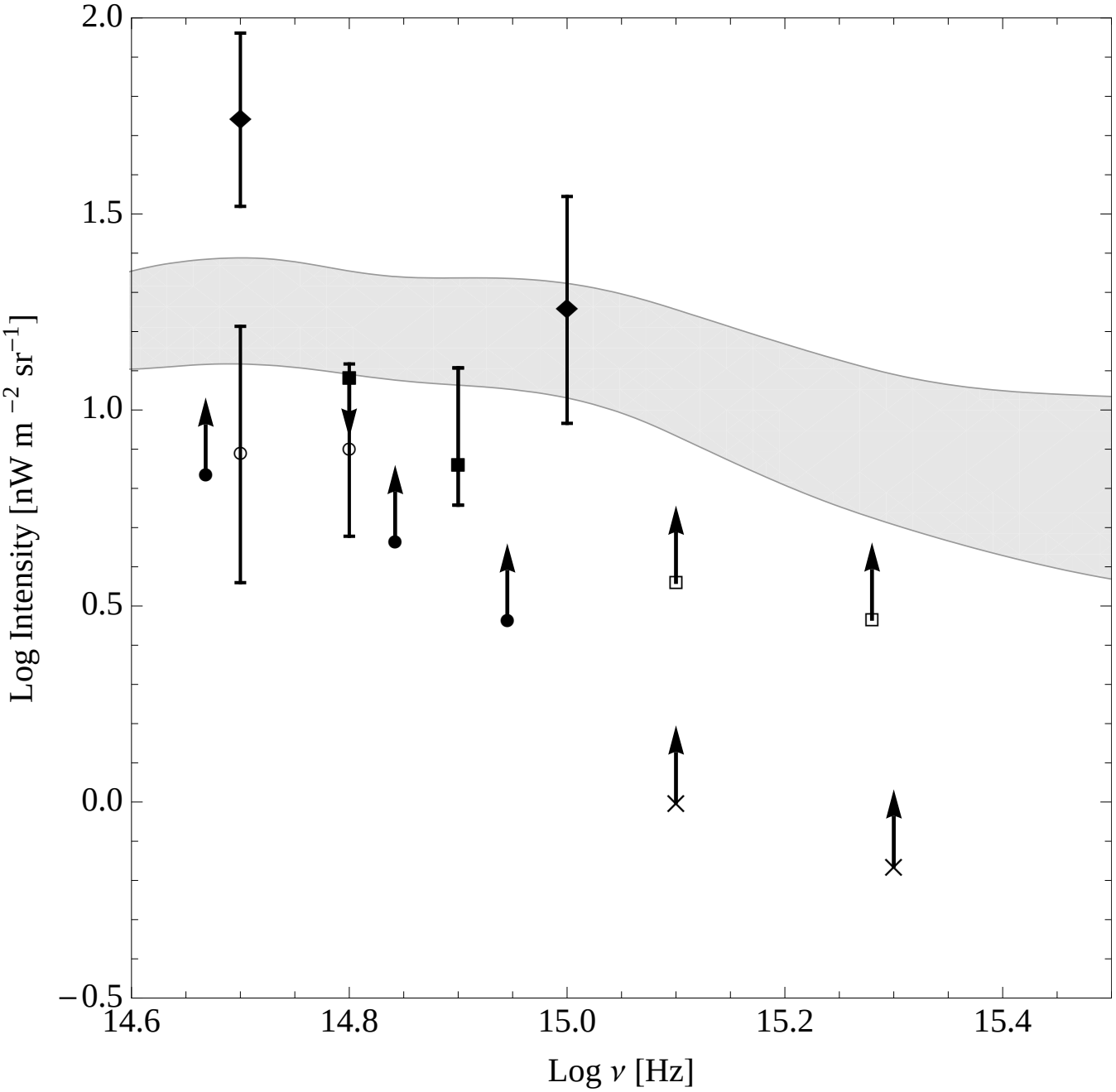
2.0
1.5
1.0
0.5
0.0
−0.5
14.6
14.8
15.0
15.2
15.4
Log Intensity [nW m $^{-2}$ sr^{-1}]
Log ν [Hz]

Figure 3.

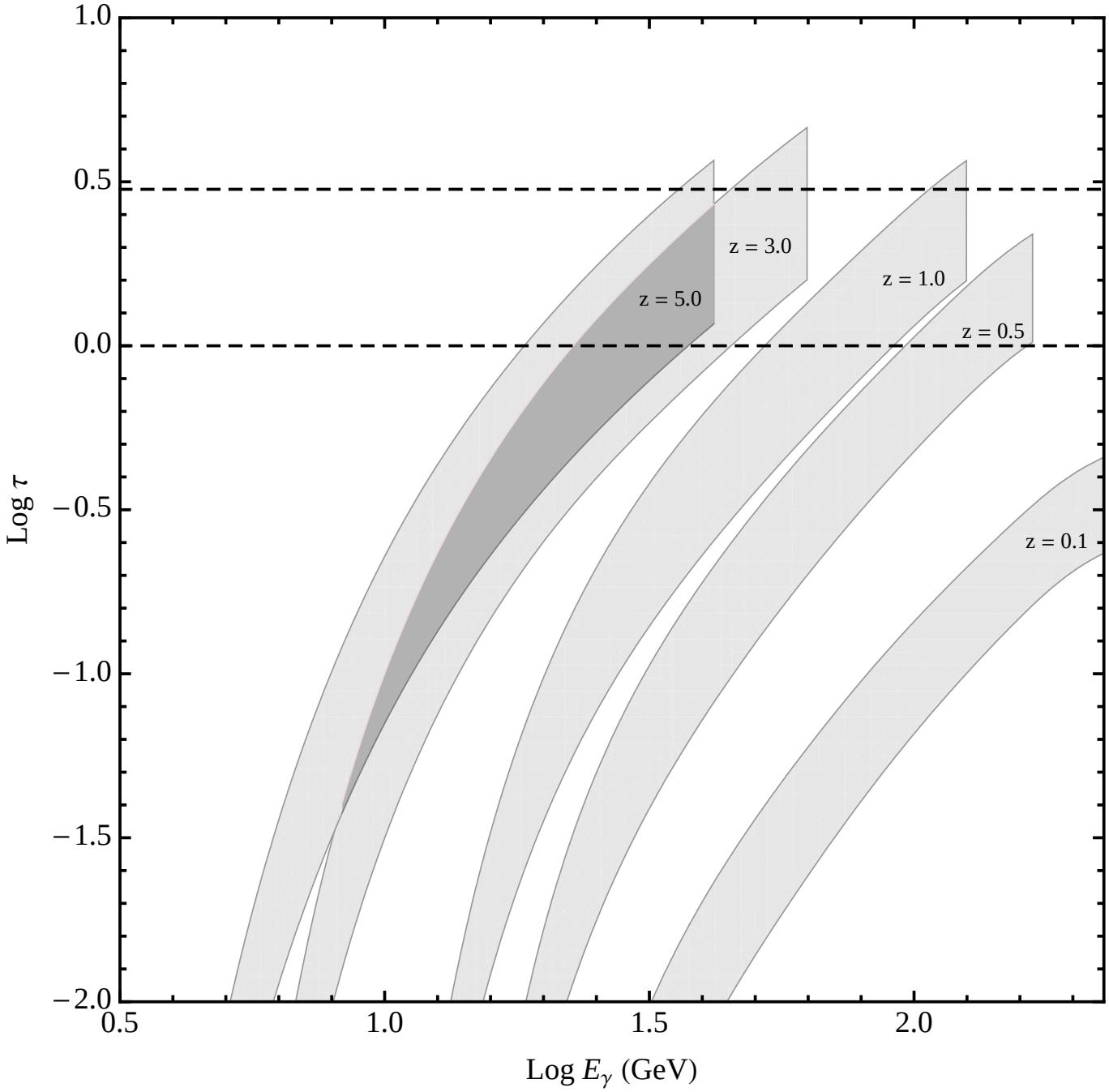
1.0
0.5
0.0
−0.5
−1.0
−1.5
−2.0
Log τ
0.5
1.0
1.5
2.0
Log E_γ (GeV)
z = 5.0
z = 3.0
z = 1.0
z = 0.5
z = 0.1

Figure 4.

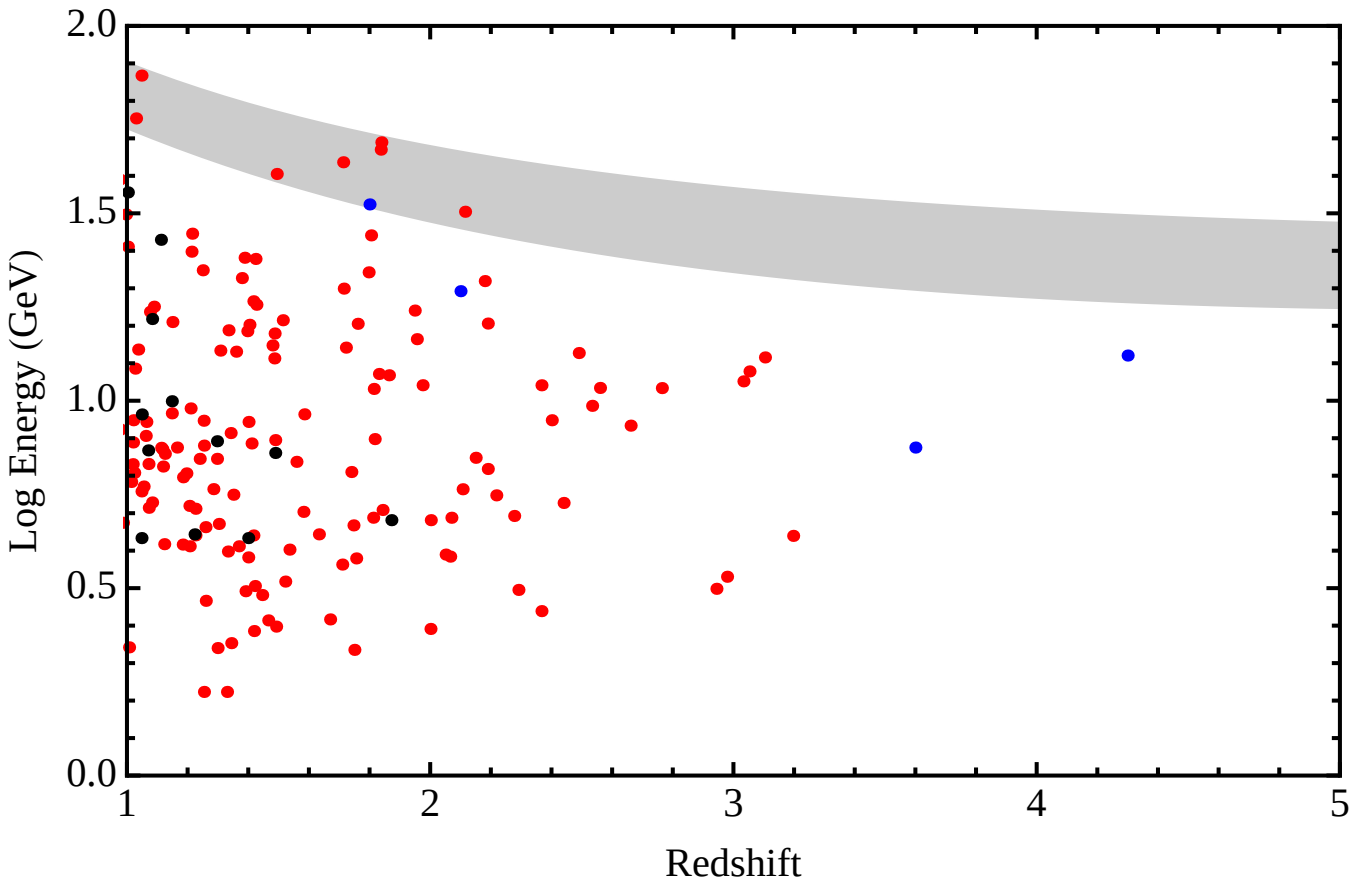

Figure 5.

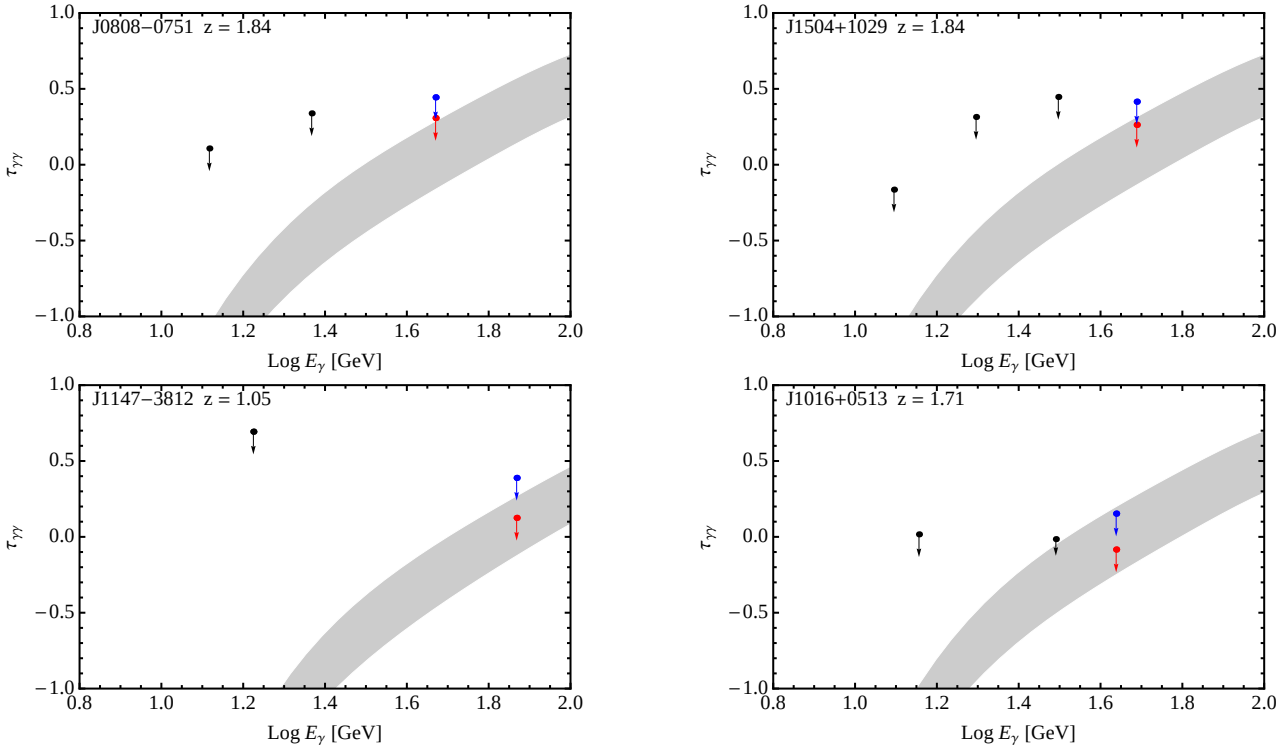
J0808−0751 z = 1.84
J1504+1029 z = 1.84
J1147−3812 z = 1.05
J1016+0513 z = 1.71
$\tau_{\gamma\gamma}$
Log E_γ [GeV]
1.0
0.5
0.0
−0.5
−1.0
0.8
1.0
1.2
1.4
1.6
1.8
2.0

Figure 6.